ELSEVIER

Computer Physics Communications 145 (2002) 48–63

Computer Physics Communications

www.elsevier.com/locate/cpc

Fitting of an ab initio potential of two linear-rigid-rotor dimer and the calculation of rovibrational energy levels by the pseudo-spectral approach

J. Castillo-Chará, John W. Bevan, Robert R. Lucchese *

Department of Chemistry, Texas A&M University, College Station, TX 77842, USA

Received 8 January 2001

Abstract

A least-squares fitting method that involves the use of the radial reproducing kernel to interpolate the radial coordinate has been applied to fit the potential of a four-dimensional linear-rigid-rotor dimer. Switching functions were used to improve the smoothness of the potential along the radial coordinate. We then use the pseudo-spectral approach to calculate the rovibrational energy levels of the dimer. For this system, the smoothed potential was tested in the calculation of the lowest eigenvalue. An observed increase in the rate of convergence as a function of the number of radial grid points and basis functions was compared to that of the unsmoothed reproducing kernel. The calculated eigenvalues were also found to converge exponentially as a function of the number of iterations. The negative of $\log_{10}$ of relative uncertainty, $|(E_\tau - E_0)/E_0|$, for the energy of the lowest eigenvalue and the negative of $\log_{10}$ of tolerance, follow a linear relationship, where relative uncertainties between 10^{-6} and 10^{-10} can be obtained, when tolerances between 10^{-6} and 10^{-10} are used in the calculation. © 2002 Published by Elsevier Science B.V.

1. Introduction

A systematic method of obtaining information about the nature of weak forces in a two linear-rigid-rotor dimer, is to construct a potential energy surface (PES), from which accurate predictions of the spectra can be made. One approach commonly used is to assume that the potential can be parametrically represented using a reduced number of characteristic parameters [1,2]. The assumed potential is then used to predict the spectrum, which by comparison with the experimental spectrum, can allow one to determine the important parameters [1–4]. The second approach is a more theoretical one, in which the PES used to solve the quantum dynamical problem of calculating the rovibrational spectrum, is calculated from first principles by ab initio theory [5–7]. By itself, this is not an easy task, since it also involves constructing an accurate analytical or global representation of the potential, which can then be used in rovibrational energy calculations. This approach has been extensively used in the calculation of rovibrational energy levels of the $(HF)_2$ dimer [8–11]. For this system, the first fitting of calculated points to an

* Corresponding author.
E-mail address: lucchese@mail.chem.tamu.edu (R.R. Lucchese).

0010-4655/02/$ – see front matter
PII: S0010-4655(02)00146-7

analytical functional form was carried out by Alexander and DePristo [12]. After this seminal work, different least-squares fits of the data to sophisticated functional forms have been undertaken [10,13,14]. For the $(HF)_2$ and $(HCl)_2$ dimers, the strength and weakness of this approach has been demonstrated. In the particular case of the $(HCl)_2$ dimer [3,4,15], the fitting of points to analytical models has allowed for the test of how accurate the functional form can reproduce the original points. Recently, Saykally and coworkers [3,4] have discussed the importance of very accurate analytical models to accurately predict the angular-radial coupling and the contraction of the intermonomer R_{CM} distance at the transition state of the $(HCl)_2$ dimer. A good description of the angular-radial coupling along the minimum energy path [3,4] is of great importance in characterizing the shape and height of the potential energy barrier for the H interchange motion characteristic of the $(HX)_2$ systems (X = F, Cl, Br, I). Since the electron density distribution of the HX diatom becomes less spherical as we go from F to I, the angular-radial coupling is expected to be even more important for the latter members of the series. Therefore, this implies the use of very sophisticated analytical models to reproduce accurately the details of the PES.

An alternative way to address the problem of the global representation of the potential is to abandon completely fitting techniques and to use interpolation approaches to globally represent the potential. However, interpolation schemes such as spline techniques require a very dense grid of points to accurately solve the problem [16], which make this approach very unappealing. Recently Rabitz and coworkers [16,17] have proposed a multidimensional interpolation scheme to globally interpolate PESs obtained from ab initio calculated points. They have shown that, this technique allows one to reproduce the asymptotic and symmetry properties of the PESs, and to increase the accuracy of the interpolated potential in the region of interest by increasing the number of points.

To illustrate the utility of this method, we will consider a global representation of the $(HBr)_2$ dimer intermolecular potential. This potential was calculated with second order Möller–Plesset perturbation theory (MP2) and 6-311++G(3pd, 3df) basis sets, and was fitted using a combined least-squares interpolation approach. Due to the fact that the intermolecular potential is very sensitive to the radial coordinate near the minimum, we will make use of the Rabitz interpolation technique [17] to interpolate the potential along the radial coordinate. The angular part will be fitted to the spherical expansion by the standard least-squares fitting procedure.

In order to calculate the rovibrational energy levels from the fitted dimer potential, we will make use of the treatment of non-direct product basis of Corey and Lemoine [18–20], and a pseudo-spectral approach similar to that used by Leforestier, and coworkers [21,22] in the calculation of vibration-rotation tunneling (VRT) states of water dimer. The basic idea behind pseudo-spectral methods is that the Hamiltonian can be evaluated using two different wave function representations [21,23–25] in which the differential and coordinate operators are respectively diagonal. In the spectral representation, the wave function is expanded as a linear combination of a finite number of well behave orthonormal polynomial functions of continuous coordinates x [25,26]. On the other hand in grid representation, the wave function is expanded in the discrete Hilbert's space as a linear combination of orthonormal polynomials evaluated at discrete points x_α, which are the eigenvalues of the coordinate operator x [25,26]. The spectral representation (momentum representation) is used to evaluate the differential operators, while the grid representation is used to evaluate the coordinate operators such as the potential.

Transformations between the two wave function representations can be carried out by unitary transformations such as the fast Fourier transform (FFT) [24] or transformations using orthogonal matrices constructed from orthogonal polynomials [20,24]. Making use of these transformation matrices, the total Hamiltonian can be evaluated accurately in a spectral representation. One of the bottle-necks in the pseudo-spectral approach is the assignment of the appropriate grid to a non-direct product of basis. Recently, Corey and Lemoine [18–20] have proposed a solution to this problem. Their idea consists of formulating a direct grid product from a non-direct product of spectral basis. By choosing the same θ grid for all values of m and using the abcisas x_α and the weights w_α of the Gauss–Legendre's quadrature, the proper two-dimensional grid $(\theta_\alpha, \varphi_q)$ for the non-direct product spectral basis composed of the spherical harmonics $Y_{lm}(\theta, \varphi)$ can be obtained. A similar treatment of a non-direct product spectral basis have been proposed by Leforestier [21,22] using Wigner rotation functions. This treatment uses the finite basis representation, and uses more grid points than basis functions. And thus this approach is equivalent to the least-squares method of Friesner [27] to evaluate the matrix elements of the potential.

In recent applications this treatment has been applied in calculations of rovibrational energy levels of Ar–H_2O and $(H_2O)_2$ dimers [22,28].

To diagonalize the Hamiltonian, the Lanczos' algorithm is the most commonly preferred choice for two principal reasons. First, because of the iterative nature of Lanczos procedures [29,30], the Hamiltonian does not need to be stored as a whole to calculate the eigenvalues. This constitutes a considerable computational advantage over direct methods that demand the storing of the Hamiltonian [29,30]. Since the sparsity of the matrix to be diagonalized is inversely related to the number of operations required per Lanczos iteration [29], very large sparse Hamiltonian matrices can be conveniently diagonalized using the Lanczos algorithm [30]. The second issue is related to the fact that the matrix–vector multiplication is basically the only operation that uses the full Hamiltonian matrix in the diagonalization process [25,29,30]. The use of the Lanczos method then avoids the alteration of the sparsity property of the Hamiltonian during the diagonalization procedure. This feature is very important since it allows for the construction of an algorithm which takes advantage of the sparsity property in all matrix–vector multiplications involved in the diagonalization process.

This paper has been divided in two main parts. In the first part, a discussion of the fitting of the potential for a two-rigid rotor dimer using least-squares interpolation technique will be presented. As an example of this procedure, we will discuss the fitting of the potential of the $(HBr)_2$ dimer, calculated at the MP2 level of theory and using the 6-311++G(3pd, 3df) basis set. In the second part, the calculation of rovibrational energy levels for this system using the pseudo-spectral approach and the impact of the radial fitting function on the convergence of the eigenvalues will be discussed.

2. Fitting of the potential

In the "two-angle embedded frame" [5,31], the interaction potential of the system can be expressed in terms of the internal coordinates $(R_{\mathrm{CM}}, \theta_A, \theta_B, \phi)$. In this set of coordinates, also called Jacobi coordinates, R_{CM} is the distance between the centers of masses of the two monomers and describes the stretching motion of the dimer. The angles θ_A and θ_B describe the orientation of monomers A and B with respect to the dimer frame, i.e. with respect to the axis containing the center of masses of the two monomers, and ϕ is the dihedral angle that describes the relative internal orientation of the two monomers about the intermonomer axis.

In order to have a global representation of the PES of the $(HBr)_2$ dimer, the calculated points at each value of R_j were fitted to the spherical expansion [32,33]

$$V(R_j, \theta_A, \theta_B, \phi) = \sum_{\Lambda} v_{\Lambda j} A_{\Lambda}(\theta_A, \theta_B, \phi), \tag{1}$$

where Λ is a collective symbol for $\{L_A, L_B, L\}$, $v_{\Lambda j}$ are the expansion coefficients [34] and $A_{\Lambda}(\theta_A, \theta_B, \phi)$ is given by

$$\begin{aligned} A_{\Lambda}(\theta_A, \theta_B, \phi) = {} & \sum_{M=0}^{\min(L_A, L_B)} (-1)^M (2 - \delta_{M,0}) \langle L_A, M; L_B, -M | L, 0 \rangle \left[\frac{(L_A - M)!(L_B - M)!}{(L_A + M)!(L_B + M)!} \right]^{1/2} \\ & \times P_{L_A}^{|M|}(\cos\theta_A) P_{L_B}^{|M|}(\cos\theta_B) \cos(M\phi), \end{aligned} \tag{2}$$

where $P_L^{|M|}(\cos\theta)$ stands for the associated Legendre polynomials [35]. The $v_{\Lambda j}$ coefficients were evaluated using the standard least-squares procedure [12], by minimizing

$$I = \sum_{\alpha} W_{\alpha} \left(V(R_j, \theta_{A,\alpha}, \theta_{B,\alpha}, \phi_{\alpha}) - \sum_{\Lambda} v_{\Lambda j} A_{\Lambda}(\theta_{A,\alpha}, \theta_{B,\alpha}, \phi_{\alpha}) \right)^2, \tag{3}$$

where W_α stands for the weights of the ab initio points in the fitting. In a final step, the four-dimensional potential was obtained by interpolating the angular potential on the grid of R_j points at fixed angular coordinates $(\theta_A^f, \theta_B^f, \phi^f)$ using a one-dimensional radial reproducing kernel [17] of the form

$$V(R, \theta_A, \theta_B, \phi) = \sum_i \alpha_i(\theta_A, \theta_B, \phi) q(R_i, R), \tag{4}$$

where $q(R_i, R)$ is the one dimensional radial reproducing kernel of the Hilbert space (RKHS) [17], and

$$\alpha_j(\theta_A, \theta_B, \phi) = \sum_{i,\Lambda} A_\Lambda(\theta_A, \theta_B, \phi) v_{\Lambda i} (m^{-1})_{ij} \quad \text{for } j = 1, 2, \ldots, N_R, \tag{5}$$

where $(m^{-1})_{ij}$ is the inverse matrix of $q(R_i, R_j)$ the one-dimensional distance-like reproducing kernel, N_R is the number of radial points, and the index i runs over the interpolated R_i points. In order to avoid unwanted discontinuities of the third and high order derivatives of the potential due to the corresponding discontinuities of the $\{q(R, R_i)\colon i = 1, \ldots, N\}$ functions, we have made use of the switching function in the kernel expression [36]. This modification allows one to obtain smoothed $q_1(R, R_i)$ fitting functions. We used a smoothed distance-like RKHS fitting function of the form [36]

$$q_1^{n=2,m=6}(R, R', \Delta R) = \frac{1}{14R^7}\left\{1 - \frac{7R'}{9R}\right\} W(R, R', \Delta R) + \frac{1}{14R'^7}\left\{1 - \frac{7R}{9R'}\right\}\left[1 - W(R, R', \Delta R)\right], \tag{6}$$

where W is a switching function defined as [37]

$$W(R, R', \Delta R) = \frac{\exp[\beta(R, R', \Delta R)]}{\exp[-\beta(R, R', \Delta R)] + \exp[\beta(R, R', \Delta R)]} \tag{7}$$

and

$$\beta(R, R', \Delta R) = \lambda\left[\frac{R - R'}{\Delta R} + \left(\frac{R - R'}{\Delta R}\right)^3\right], \tag{8}$$

where we have taken $\lambda = (1/2)\tanh^{-1}(0.8)$ and where ΔR defines the range of the switching.

One of the most important concerns in the least-squares fitting procedure, was to obtain an accurate representation of the potential near the equilibrium minimum. A simple way of doing this is to use non-uniform weighted points to obtain an accurate fit in the region of interest. The points used in Eq. (3), were weighted using weights given by

$$W_\alpha = \frac{1}{1 + (V(R_j, \theta_A, \theta_B, \phi) - E_{\min})/F_w}, \tag{9}$$

where, $E_{\min}$, is the value of the potential at the minimum equilibrium distance in the PES, and F_w is the weight factor parameter. The value for this parameter was taken to be the maximum value for which, ΔV, the average value of the absolute difference between the ab initio calculated points and the potential calculated in a selected range of values of V, was less than a fixed value.

3. Fitting of the $(HBr)_2$ ab initio potential

As an example of the use of the fitting procedure explained above, we obtain a global representation of the intermolecular potential for the $(HBr)_2$ dimer, at any arbitrary point $(R, \theta_A, \theta_B, \phi)$ on the PES. An accurate representation of the intermolecular potential, was obtained using 55 $v_{L_A L_B L}$ coefficients. In our fitted potential, an average absolute difference of ΔV of less than 6 cm^{-1} was obtained using a weight factor $F_w = 50$, in the

Table 1
Average absolute difference of the fitted potential and the calculated ab initio points within 250 cm^{-1} of the minimum for the $(HBr)_2$ dimer as a function of the radial coordinate

	ΔV average absolute difference (cm^{-1})			
F_w (cm^{-1})	R_{CM}[a] = 3.50	4.00	4.50	5.00
25	5.42	5.32	4.37	2.24
50	6.30	5.81	4.73	2.25
75	7.17	6.21	5.02	2.25
100	8.03	6.63	5.29	2.25
125	8.84	6.97	5.54	2.26

[a] The center of mass separation in Å.

region near the minimum, where $R_{CM} = 4.0$ Å and well depths in the range 445 to 690 cm^{-1}, i.e. all points within 250 cm^{-1} of the minimum. In order to evaluate the reliability of the fit over the radial grid, the value of ΔV as a function of R_{CM} is shown in Table 1. This Table indicates the fact that the deviation decreases as the intermonomer distance is increased, which can be interpreted in terms of the weak dependence of the potential on the radial coordinate at larger distances. At short range, however, the potential depends strongly on the radial coordinate making the potential very stiff. This makes the fitting of the potential more difficult and consequently increases the deviation.

The radial dependence of the larger contributing coefficients $v_{L_A L_B L}$, in the region near the minimum, was analyzed by plotting the coefficients v_{000}, v_{011}, v_{033}, v_{044}, v_{022}, v_{112} and v_{224} as a function of the radial coordinate. Fig. 1 shows clearly that the larger contribution is that of the isotropic coefficient v_{000}, following in importance the v_{011} and the dipole–dipole coefficient v_{112}. The last two terms become quite strong at short range. The higher angular function coefficients v_{033} and v_{044} appear to contribute significantly at very short range as indicated in Fig. 1. The occurrence of higher angular function coefficients can be explained as due to the interaction of the non-spherical electron density distributions of the HBr monomers in the L-type equilibrium structure of the dimer. Due to this characteristic feature, higher angular functions coefficients are required to reproduce the strong angular-radial coupling at short range, when the monomer at the perpendicular position rotates.

The relative importance of the v_{033} and v_{044} coefficients can be evaluated by comparing them with the v_{112} and v_{022} coefficients. As indicated in Fig. 1, the contribution of the v_{033} is very similar to that of the dipole–dipole coefficient at short range. Similarly, v_{044} coefficient is of the same magnitude as that of the v_{022} coefficient. Since the contribution of the coefficients v_{033} and v_{044} is comparatively larger than that of the dipole–dipole coefficient v_{112}, this gives us information about the directionality of forces. This implies that non-directional forces coming from the v_{033} and v_{044} coefficients could be more important than the directional forces originated from the dipole–dipole interaction coefficient (v_{112}). This analysis explains to some extent, the L-type configuration at the equilibrium minimum structure of the $(HBr)_2$ dimer. Non-directional forces due to the contributions of higher multipole term favor the L-type configuration, while directional forces such as the dipole–dipole term favors linear type configurations that maximize this interaction.

4. Calculation of rovibrational energy levels by the pseudo-spectral approach

4.1. Hamiltonian

The rovibrational energy levels were calculated by the pseudo-spectral approach, a procedure similar to that developed by Leforestier and coworkers [22,28] to calculate rovibrational energy levels of the water dimer. For two interacting linear rigid rotors, the rovibrational dynamics of the complex can be described using the following Hamiltonian expression in the “two-angle embedded frame” [5]

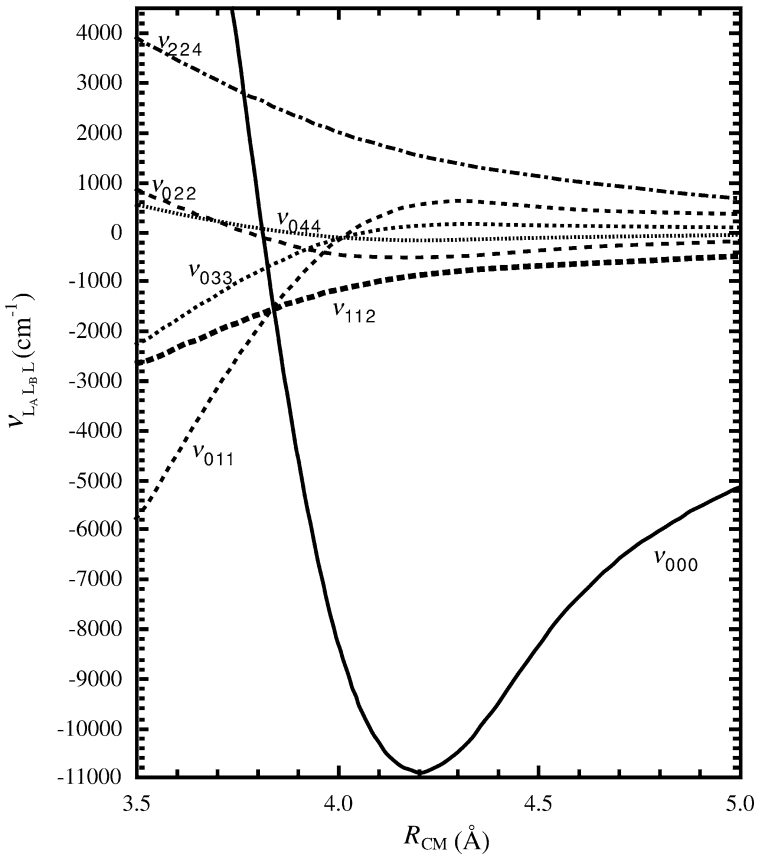

Fig. 1. Radial dependence of the larger contributing coefficients used to fit the MP2 potential of the $(HBr)_2$ dimer, obtained by interpolating the v_{Aj} coefficients along the radial grid.

$$H = \frac{-\hbar^2}{2\mu_{AB}R^2}\frac{\partial}{\partial R}R^2\frac{\partial}{\partial R} + K_A + K_B + \frac{1}{2\mu_{AB}R^2}\left[J^2 + j^2 - j\cdot J\right] + V(R_{CM},\theta_A,\theta_B,\phi), \tag{10}$$

where K_A and K_B represent the kinetic energy expressions for the rotational motion of monomers with rotational angular momenta j_A and j_B, respectively. The internal angular momentum, j, is given by

$$\vec{j} = \vec{j}_A + \vec{j}_B, \tag{11}$$

the vector sum of the rotational angular momenta of the monomers. The total angular momentum of the system, J, is related to the internal (j) and end-over-end angular momentum (ℓ) by

$$\vec{J} = \vec{\ell} + \vec{j}. \tag{12}$$

In the pseudo-spectral approach followed in this paper, the Hamiltonian was split into six contributing terms as follows:

$$H_{BF} = K_A + K_B + T_R + T_{DD} + H_{OCC} + V(R,\theta_A,\theta_B,\phi), \tag{13}$$

where

$$T_R = \frac{-\hbar^2}{2\mu_{AB}R^2}\frac{\partial}{\partial R}R^2\frac{\partial}{\partial R}, \tag{14}$$

$$T_{\mathrm{DD}} = \frac{1}{2\mu R^2}\left[\left(J^{\mathrm{SF}}\right)^2 + j^2 - 2j_z J_z\right], \tag{15}$$

and

$$H_{\mathrm{OCC}} = \frac{-1}{2\mu_{AB} R^2}[j_+ J_+ + j_- J_-]. \tag{16}$$

The T_R term represents the kinetic energy for the stretching motion, T_{DD} describes the kinetic energy of the dimer considered as a pseudo diatom and H_{OCC} represents the off-diagonal Coriolis interaction terms. Since the H_{OCC} are generally very small, we have neglected these terms in our calculations.

A prolate symmetric top convention [38] is used to describe the monomeric principal moments of inertia (orientating the a-principal axis along the z-axis). If the monomers intramolecular distances are fixed, the monomer Hamiltonians H_A and H_B reduce to their respective kinetic energy expressions K_A and K_B, as given below

$$H_A = K_A = B_{eA}(j_A)^2 \quad \text{and} \quad H_B = K_B = B_{eB}(j_B)^2, \tag{17}$$

where the B_e are the equilibrium rotational constants.

4.2. Wave function representations

For a dimer formed from two interacting rigid linear molecules, the total wave function can be expanded as a linear combination of radial and angular momentum products [33,39] using a basis set of the form

$$\begin{aligned}&\langle \hat{r}, \widehat{R}, \gamma, R | n, j_A, j_B, j, K; J, M\rangle \\ &\quad = S_n(R)\left[\frac{(2J+1)}{4\pi}\right]^{1/2} \sum_{m_A m_B} Y_{j_A m_A}(\theta_A, 0) y_{j_B m_B}(\theta_B, 0) \mathrm{e}^{\mathrm{i}\frac{w}{2}\phi} \langle j_A m_A; j_B m_B | j K\rangle D^{(J)}_{MK}(\alpha, \beta, \gamma)^*,\end{aligned} \tag{18}$$

where $\hat{r} = (\theta_A, \theta_B, \phi)$ and $\widehat{R} = (\alpha, \beta, \gamma)$, $Y_{j_A m_A}(\theta_A, 0)$ and $y_{j_B m_B}(\theta_B, 0)$ are the spherical harmonics [35], $D^{(J)}_{MK}(\alpha, \beta, \gamma)^*$ is the rotation matrix [40], and $\langle j_A m_A; j_B m_B | j K\rangle$ are the Clebsch–Gordan coefficients. The radial basis functions are given by

$$S_n(R) = \frac{1}{R}\sqrt{\frac{2}{L}} \sin\frac{n\pi(R - R_{\mathrm{start}})}{L}, \quad L = R_{\mathrm{end}} - R_{\mathrm{start}} \tag{19}$$

and R_{end} and R_{start} are the last and first points of the radial grid. We have also used in Eq. (18) the transformation

$$m_A\phi_A + m_B\phi_B = \left(\frac{1}{2}\right)(\phi_A + \phi_B)(m_A + m_B) + \left(\frac{1}{2}\right)(\phi_A - \phi_B)(m_A - m_B), \tag{20}$$

where $K = m_A + m_B$, $w = m_A - m_B$, $\gamma = (\frac{1}{2})(\phi_A + \phi_A)$, and $\phi = \phi_A - \phi_B$. The γ angle describes the overall rotations of two rotors, the ϕ angle describes the internal rotation motion, K and w are respectively the quantum numbers that account for the overall and internal rotational motion of the two rotors. After the transformation, a factor containing γ in the transformed basis allows the proper evaluation of the action of the J^2 operator, in the transformed coupled basis in a straight forward manner.

After parity adaptation [33,41], the basis set for the coupled wave function is given by

$$\begin{aligned}&\langle \hat{r}, \widehat{R}, \gamma, R | n, j_A, j_B, j, K; \varepsilon, J, M\rangle \\ &\quad = S_n(R)\left[\frac{(2J+1)}{8\pi}\right]^{1/2} \left(\Upsilon^{jK}_{j_A j_B}(\hat{r}) D^{(J)}_{MK}(\alpha, \beta, \gamma)^* - \varepsilon P \Upsilon^{j-K}_{j_A j_B}(\hat{r}) D^{(J)}_{M-K}(\alpha, \beta, \gamma)^*\right).\end{aligned} \tag{21}$$

The coefficient $\varepsilon = \pm 1$ is the wave function parity and the effect of the parity operator P on the basis is given by

$$P\Upsilon^{jK}_{j_A j_B}(\hat{r}) D^{(J)}_{MK}(\alpha, \beta, \gamma)^* = (-1)^{J + j_A + j_B + j} \Upsilon^{jK}_{j_A j_B}(\hat{r}) D^{(J)}_{MK}(\alpha, \beta, \gamma)^*$$

and

$$\Upsilon^{jK}_{j_A j_B}(\theta_A,\theta_B,\phi)=\sum_{m_A m_B}\langle j_A,m_A,j_B,m_B|j,K\rangle Y_{j_A m_A}(\theta_A,0)Y_{j_B m_B}(\theta_B,0)\mathrm{e}^{\mathrm{i}\frac{w}{2}\phi}. \tag{22}$$

In order to obtain the grid representation of the total wave function, we start with the uncoupled spectral wave function representation expanded as [22]

$$\langle R,\theta_A,\theta_B,\phi,\widehat{R}|\Psi\rangle=\sum_{j_A j_B m_A+m_B=K}\Psi^{JM}_{j_A m_A j_B m_B n}X^{JM}_{j_A m_A j_B m_B}(\theta_A,\theta_B,\phi)S_n(R)\langle\alpha,\beta,\gamma|J,K,M\rangle. \tag{23}$$

Eq. (23) may also be written in bra-ket notation as

$$\left|\Psi^{JM}_{\mathrm{u}}\right\rangle=\sum_{j_A j_B m_A+m_B=K}\Psi^{JM}_{nj_A m_A j_B m_B}|n,j_A,m_A,j_B,m_B,J,M\rangle, \tag{24}$$

where $\langle R,\theta_A,\theta_B,\phi|n,j_A,m_A,j_B,m_B,J,K,M\rangle=S_n(R)X^{JM}_{j_A m_A j_B m_B}(\theta_A,\theta_B,\phi)\langle\alpha,\beta,\gamma|J,K,M\rangle$. In these expressions $\Psi^{JM}_{nj_A m_A j_B m_B}$ is the wave function vector expansion coefficient and $X^{JM}_{j_A m_A j_B m_B}$ is given by

$$\begin{aligned}X^{JM}_{j_A m_A j_B m_B}(\theta_A,\theta_B,\phi)\;=\;&(-1)^{(m_A+m_B+|m_A|+|m_B|)/2}\left[\frac{(j_A-|m_A|)!(j_B-|m_B|!)}{(j_A+|m_A|)!(j_B+|m_B|)!}\right]^{(1/2)}\\&\times P^{|m_A|}_{j_A}(\cos\theta_A)P^{|m_B|}_{j_B}(\cos\theta_B)\mathrm{e}^{\frac{1}{2}\mathrm{i}w\phi}.\end{aligned} \tag{25}$$

The first step in the transformation of the uncouple spectral basis, Eq. (24), is the transformation of, $\Psi^{JM}_{nj_A m_A j_B m_B}$, the vector of expansion coefficients for the wave function, from radial spectral basis $S_n(R)$ to a radial grid, by using the inverse fast Fourier transform (IFFT) [20,22]

$$\Psi^{JM}_{pj_A m_A j_B m_B}=\sum_n F^{(R)+}_{np}\Psi^{JM}_{nj_A m_A j_B m_B}, \tag{26}$$

where $F^{(R)+}_{np}$ is the IFFT matrix given by

$$F^{(R)+}_{np}=\frac{\mathrm{e}^{-\mathrm{i}K_n R_p}}{(N_R)^{1/2}}\quad\text{and}\quad K_n=\frac{2n\pi}{N_R\Delta R}, \tag{27}$$

and where N_R is the number of points used in the radial grid and ΔR is the step size. In the second step, we transform the spectral representation of j_A and j_B applying the orthonormal matrices [22] $R^{(m_A)}_{\alpha j_A}$ and $R^{(m_B)}_{\beta j_B}$ to the wave function vector coefficient $\Psi^{JM}_{pj_A m_A j_B m_B}$ obtained in the first step. The total transformation is given by

$$\Psi^{JMK}_{p\alpha\beta w}=\sum_{j_A,j_B,m_A+m_B=K}R^{(m_A)}_{\alpha j_A}R^{(m_B)}_{\beta j_B}\Psi^{JM}_{pj_A m_A j_B m_B}. \tag{28}$$

This transformation is carried out for all allowed values of m_A and m_B that satisfy [22]

$$K=m_A+m_B,\quad w=m_A-m_B, \tag{29}$$

and all allowed K values for a given total angular momentum J with $|K|\leqslant J$. In Eq. (28) $R^{(m_A)}_{\alpha j_A}$ and $R^{(m_B)}_{\beta j_B}$ are the orthonormal matrices given by [22]

$$R^{(m_A)}_{\alpha j_A}=\sqrt{w_\alpha}P^{|m_A|}_{j_A}(\cos\theta_\alpha)\quad\text{and}\quad R^{(m_B)}_{\beta j_B}=\sqrt{w_\beta}P^{|m_B|}_{j_B}(\cos\theta_\beta). \tag{30}$$

Here w_α and w_β represents the Gauss–Legendre quadrature weights, α and β represent the points used in the transformations [42]. In a final step, the total grid representation is obtained by the IFFT of the $\Psi^{JMK}_{p\alpha\beta w}$ coefficient over the allowed values of K and w quantum numbers by the following expression

$$\Psi^{JMK}_{p\alpha\beta q} = \mathrm{e}^{\frac{1}{2}\mathrm{i}w_{\min}\phi} \sum_{w} F^{(\phi)+}_{qw(w')} \Psi^{JMK}_{p\alpha\beta w(w')}, \tag{31}$$

where

$$F^{(\phi)+}_{qw(w')} = \frac{\mathrm{e}^{\mathrm{i}\phi w'}}{(N_\phi)^{1/2}} \quad \text{and} \quad \phi = \frac{2q\pi}{(N_\phi+1)}. \tag{32}$$

The actual number of points used in the transformation is $N_\phi + 1$ and the index q takes the values $0, 1, 2, \ldots, N_\phi$. In this transformation w and w' are related through

$$w = w_{\min} + 2w', \tag{33}$$

and $w_{\min} = \max(-2m_A + \Omega, -2m_B - \Omega)$. With the relationship in Eq. (33), the coefficients can be transformed by using the standard IFFT without separating the even and odd symmetries.

4.3. Matrix element evaluations

Using the partition of the Hamiltonian given in Eq. (13), the matrix elements of the first three terms can be evaluated directly in the total coupled spectral representation $|\Psi^{JM}_c\rangle$, in which they are diagonal. Operating the respective operators onto this representation, the eigenvalues are given by [22,31,33]

$$(K_A + K_B + T_R)\big|\Psi^{JM}_c\big\rangle = \sum_{nj_Aj_Bj K} \kappa^{JKM}_{nj_Aj_Bj} |S_n\rangle|j_A, j_B; j, K\rangle|J, K, M\rangle, \tag{34}$$

where

$$\big|\Psi^{JM}_c\big\rangle = \sum_{nj_Aj_BjK} \Psi^{JM}_{nj_Aj_BjK} |S_n\rangle|j_A, j_B; j, K\rangle|J, K, M\rangle \tag{35}$$

and

$$\kappa^{JKM}_{nj_Aj_Bj} = \hbar^2\left[B_{eA} j_A(j_A+1) + B_{eB} j_B(j_B+1) + \frac{2(n-1)^2\pi^2}{\mu_{AB}L^2}\right]\Psi^{JM}_{nj_Aj_BjK} \tag{36}$$

with $L = R_{\text{end}} - R_{\text{start}}$, $n = 1, 2, \ldots, N_R$. Without taking into account the $1/(2\mu_{AB}R^2)$ factor, the T_{DD} is diagonal in total coupled representation. The proper evaluation of this term can be carried out in the mixed representation

$$\big|\Psi^{JM}_{\text{mix}}\big\rangle = \sum_{pj_Aj_BjK} \Psi^{JM}_{pj_Aj_BjK} |R_p\rangle|j_A, j_B; j, K\rangle|J, K, M\rangle, \tag{37}$$

where the radial wave functions $|R_p\rangle$ are the delta functions located at evenly spaced points R_p with $p = 1, 2, \ldots, N_R$. In this representation the action of the T_{DD} operator can be evaluated as follow:

$$T_{\text{DD}}\big|\Psi^{JM}_{\text{mix}}\big\rangle = \sum_{pj_Aj_BjK} \lambda^{JM}_{pj_Aj_BjK} |R_p\rangle|j_A, j_B; j, K\rangle|J, K, M\rangle, \tag{38}$$

where

$$\lambda^{JM}_{pj_Aj_BjK} = \left(\frac{\hbar^2}{2\mu_{AB}R_p^2}\right)\big[J(J+1) + j(j+1) - 2K^2\big]\Psi^{JM}_{pj_Aj_BjK}. \tag{39}$$

The remaining term in our split Hamiltonian is the potential. This term can be evaluated using the total grid representation $|R_p\rangle|\theta_{A\alpha}\rangle|\theta_{B\beta}\rangle|\phi_q\rangle|J, K, M\rangle$, by evaluating the potential at each grid point of the total grid representation [21,22]. Since the potential matrix elements are diagonal in the total grid representation, we can write

$$V\big|\Psi^{JM}_G\big\rangle = \sum_{p\alpha\beta q} \chi^{JMK}_{p\alpha\beta q} |R_p\rangle|\theta_{A\alpha}\rangle|\theta_{B\beta}\rangle|\phi_q\rangle|J, K, M\rangle, \tag{40}$$

where

$$\left|\Psi_G^{JM}\right\rangle = \sum_{p\alpha\beta q} \Psi_{p\alpha\beta q}^{JMK} |R_p\rangle|\theta_{A\alpha}\rangle|\theta_{B\beta}\rangle|\phi_q\rangle|J, K, M\rangle \tag{41}$$

and

$$\chi_{p\alpha\beta q}^{JMK} = V(R_p, \theta_{A\alpha}, \theta_{B\beta}, \phi_q)\Psi_{p\alpha\beta q}^{JMK}. \tag{42}$$

Since the off-diagonal Coriolis coupling operator H_{OCC} defined in Eq. (16) can be represented by analytical expressions in the coupled angular basis $|\Psi_c^{JM}\rangle$ [22], its matrix elements can be evaluated using the mixed representation $|R_p\rangle|j_A, j_B; j, K\rangle|J, K, M\rangle$, following the same procedure used in the evaluation of T_{DD}. However, in our calculations, we make use of the helicity decoupling approximation [33], for which the contribution of this term has been neglected. After every term of our split Hamiltonian has been evaluated in the appropriate representation, we transform the vectors $\lambda_{p,j_A,j_B,jK}^{JM}$ and $\chi_{p,\alpha,\beta,q}^{JM}$ back to the coupled representation given in Eq. (18). Using the respective transformation matrices, this step is accomplished by

$$\lambda_{n,j_A,j_B,j}^{JMK} = \sum_p F_{np}^{(R)} \lambda_{pj_A j_B jK}^{JM} \tag{43}$$

and

$$\chi_{n,j_A,j_B,j}^{JMK} = \sum_{m_A} T_{jm_A} \sum_p F_{np}^{(R)} \sum_\alpha R_{\alpha j_A}^{(m_A)} \sum_\beta R_{\beta j_B}^{(m_B)} \mathrm{e}^{-\frac{1}{2}\mathrm{i}\phi w_{\min}} \sum_q F_{w(w')q}^{(\phi)} \chi_{p\alpha\beta q}^{JM} \tag{44}$$

transformations. Where $\lambda_{n,j_A,j_B,j}^{JMK}$ and $\chi_{n,j_A,j_B,j}^{JMK}$ represent the wave function vector coefficients in the coupled spectral basis and T_{jm_A} is the matrix transformation from the uncoupled to the coupled representation using the Clebsch–Gordan coefficients. The total representation of the Hamiltonian operator in the coupled spectral basis is given by

$$H\left|\Psi_c^{JM}\right\rangle = \sum_{n,j_A,j_B,j,K} \left(\kappa_{n,j_A,j_B,j}^{JMK} + \lambda_{n,j_A,j_B,j}^{JMK} + \chi_{n,j_A,j_B,j}^{JMK}\right)|n, j_A, j_B, j, K, J, M\rangle \tag{45}$$

in terms of the basis set defined in Eq. (18). Given this procedure for computing $H|\Psi_c^{JM}\rangle$ from an arbitrary initial guess vector $|\Psi_c^{JM}\rangle$, we can then obtain the eigenvalues and eigenvectors of H using the Lanczos method [30,43] discussed in the next section.

4.4. Rovibrational energy levels

In the Lanczos's diagonalization procedure, a tridiagonalized representation of the Hamiltonian in spectral representation using the Lanczos algorithm is obtained [30,43]. Starting with an initial vector $|q_0\rangle$ in the coupled representation, the diagonal and off-diagonal matrix elements of the tridiagonal matrix T_n are iteratively generated. Where

$$T_n = \begin{bmatrix} \langle q_1| \\ \vdots \\ \langle q_n| \end{bmatrix} \left[H|q_1\rangle, \quad \ldots, \quad H|q_n\rangle\right] = \begin{bmatrix} a_1 & b_1 & & \\ b_1 & a_2 & b_2 & \\ & b_2 & . & . \\ & & . & a_n \end{bmatrix}, \tag{46}$$

the diagonal elements a_i are given by $a_i = \langle q_i|H|q_i\rangle$, and the off-diagonal matrix elements b_i by $b_i = \langle q_{i+1}|H|q_i\rangle$, respectively. In the final step, the eigenvalues were calculated by diagonalizing the tridiagonal matrix T_n using the bisection algorithm.

5. Convergence of the eigenvalues

Given a global representation of the interaction potential for a two-rigid rotor system, the method detailed in the previous section can be used to obtain the eigenvalues of the corresponding Hamiltonian. In this procedure, there are a number of parameters, which control the accuracy of the resulting eigenvalues. The parameters are R_{end}, R_{start}, N_R, N_θ, N_ϕ, N_F, $j_{\max}$, $m_{\max}$, and τ. R_{start} is the first point of the radial grid, R_{end} is the last point, N_R is the number of grid points in the radial direction, N_θ is the number of θ_A and θ_B points used in the grid, and N_ϕ is the number of ϕ points. All of the summations over spectral states are truncated so that $j_A, j_B \leqslant j_{\max}$ and $m_A, m_B \leqslant m_{\max}$, where τ is the tolerance used to determine the convergence of the eigenvalues in the Lanczos procedure.

We have studied the convergence of the eigenvalues with respect to the outlined parameters above by again considering the $(HBr)_2$ system discussed in Section 3. In order to obtain an optimal set of parameters $(R_{\text{end}}, R_{\text{start}}, N_R, N_\theta, N_\phi, N_F, j_{\max}, m_{\max}, \tau)$ to properly diagonalize the Hamiltonian in the spectral representation, the radial limits $(R_{\text{end}}, R_{\text{start}})$ were varied systematically keeping fixed the parameters of the angular basis $j_{\max}$, $m_{\max}$, N_θ, and N_ϕ. For the $(HBr)_2$ dimer, we use a value 74670.95581 a.u. for the reduced mass and a value of 8.348460(5) cm^{-1} for the HBr monomer rotational constant [44]. This systematic optimization of the radial points $(R_{\text{end}}, R_{\text{start}})$ was carried out at $J = 0$, $j_{\max} = 8$, $m_{\max} = 8$, $N_\theta = 12$ and $N_\phi + 1 = 17$. The optimal radial limits selected, were those for which the smallest number of radial grid points were required to converge the lowest eigenvalue. As indicated in Table 2, the optimal values of R_{start}, and R_{end} in our potential were respectively 7.0 and 12.6 a.u. using $N_F = 32$ radial spectral basis functions and $N_R = 35$ radial grid points. Following the radial optimization, $j_{\max} + 1$, the number of spectral basis functions for the θ_A and θ_B coordinates ($j_{A\max} = j_{B\max} = j_{\max}$), and $2m_{\max} + 1$, the number of spectral functions for the torsional motion about (ϕ) were optimized. The energy of the lowest eigenvalue is practically independent on the number of extra grid points used to converge the eigenvalues. This reflects the fact that the global minimum in the $(HBr)_2$ potential is practically independent of the ϕ coordinate. The motion about the ϕ coordinate is important at higher energy states, such as odd parity states, where the motion about ϕ breaks the planar configuration of the dimer to perform the tunneling bending mode. Keeping all other parameters fixed, at the values displayed in Table 2, it was found after varying $j_{\max}$ and $m_{\max}$ that $j_{\max} = m_{\max} = 8$, were the lowest values, for which the ground state energy converges with uncertainty of ± 0.01 cm^{-1}. This is clearly demonstrated in the plot of the energy of the two lowest eigenvalues as a function of $j_{\max}$ given in Fig. 2. As depicted in Fig. 2, the energies of these two eigenvalues have a smooth convergence as a function of $j_{\max}$. This dependence appears to become linear at $j_{\max}$ values larger than 8, which implies that the eigenvalues converge exponentially with increasing $j_{\max}$. Note that the results in this figure implicitly assume that the result with $j_{\max} = 11$ is fully converged. Thus to demonstrate the exponential convergence for the higher values of $j_{\max}$, we would need to use as our "converged" value one obtained with a $j_{\max}$ larger than 11. Simi-

Table 2
Convergence parameters used to calculate the $(HBr)_2$ rovibrational energy levels

Parameter	Value
N_R	35
R_{start} (a.u.)	7.0
R_{end} (a.u.)	12.6
N_θ[a]	12
$N_\phi + 1$	17
N_F	32
$j_{\max}$	8
$m_{\max}$	8
τ	10^{-12}

[a] $N_\theta = N_{\theta_A} = N_{\theta_B}$ represents the number of grid points along θ_A and θ_B coordinates, respectively.

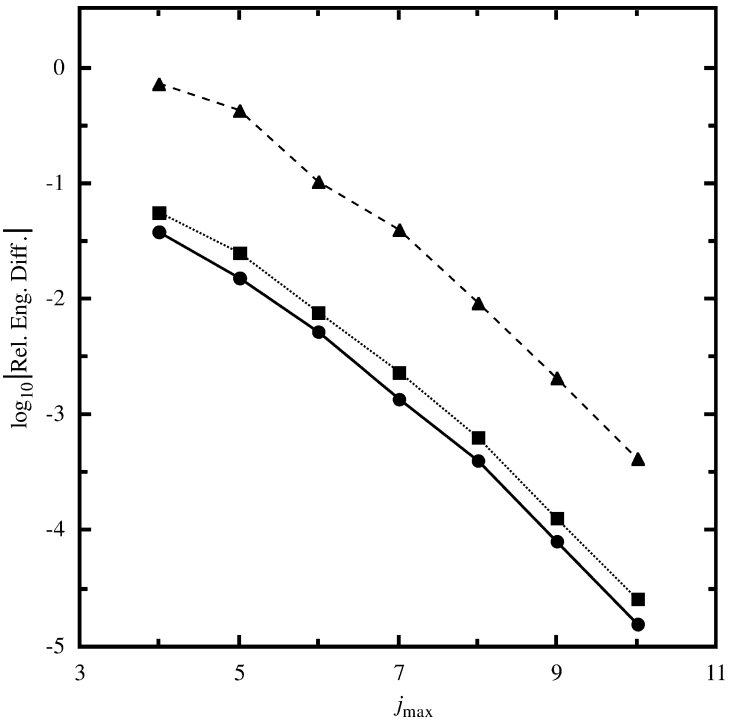

Fig. 2. Relative energy difference |Rel. Eng. Diff.| of the two lowest eigenvalues for $J = 0$ and the ground state tunneling frequency of the $(HBr)_2$ dimer, plotted on a logarithmic scale as a function of $j_{\max}$, the maximum HBr rotational quantum number. Squares represent the relative energy difference $|(E^{(1)}_{j_{\max}} - E^{(1)}_{j_{\max}=11})/E^{(1)}_{j_{\max}=11}|$ of lowest eigenvalue (+), circles the relative energy difference $|(E^{(2)}_{j_{\max}} - E^{(2)}_{j_{\max}=11})/E^{(2)}_{j_{\max}=11}|$ of the second lowest eigenvalue (−) and triangles the relative energy difference $|(\nu_5^{(j_{\max})} - \nu_5^{(j_{\max}=11)})/\nu_5^{(j_{\max}=11)}|$ for the tunneling frequency. The plus (+) and minus (−) stand for the exchange symmetry labels of the total wave function.

larly to the relative energies of the two lowest eigenvalues, the relative difference for the ground state tunneling frequency, in Fig. 2, exhibits similar slope as a function of $j_{\max}$. This implies that the calculation of this property converges in a way analogous to the convergence of the energies of the two lowest eigenvalues. The similarity in slope and the smoothness of this plot are indicative of the good stability and convergence of the calculated eigenvalues.

Along the radial coordinate, the increase in the number of grid points (decreasing the step size ΔR), keeping the remaining parameters fixed as depicted in Fig. 3, produces slow convergence of the lowest eigenvalue when the unsmooth radial reproducing kernel is used to interpolate the radial coordinate. In this figure, the number of radial functions has been fixed to 32 and the number of radial points has been varied from 32 to 220. The slow convergence of the eigenvalues is caused by the discontinuities in the third and higher order derivatives of the radial reproducing kernel. Although the use of the smooth radial reproducing kernel causes an unwanted oscillatory behavior in the convergence of the eigenvalues, this still leads to a better convergence when compared with the unsmooth case discussed above. In Fig. 4, the number of radial functions is half the number of radial points at each point of the plot. This figure illustrates clearly the fact that the use of the switching function to remove the discontinuities in the derivatives of the radial reproducing kernel, increases the rate of convergence of the lowest eigenvalue significantly, as indicated by the slopes of the plots. The optimum value for the step size was 0.162 leading a grid of 35 points.

The last optimized parameter was the tolerance (τ). Fixing all the remaining parameters in Table 2, the tolerance was varied in order to obtain a more clear understanding of the convergence of the eigenvalues as a function of the tolerance (τ). The energy of the lowest eigenvalue, E_0, was compared to the energies calculated at given

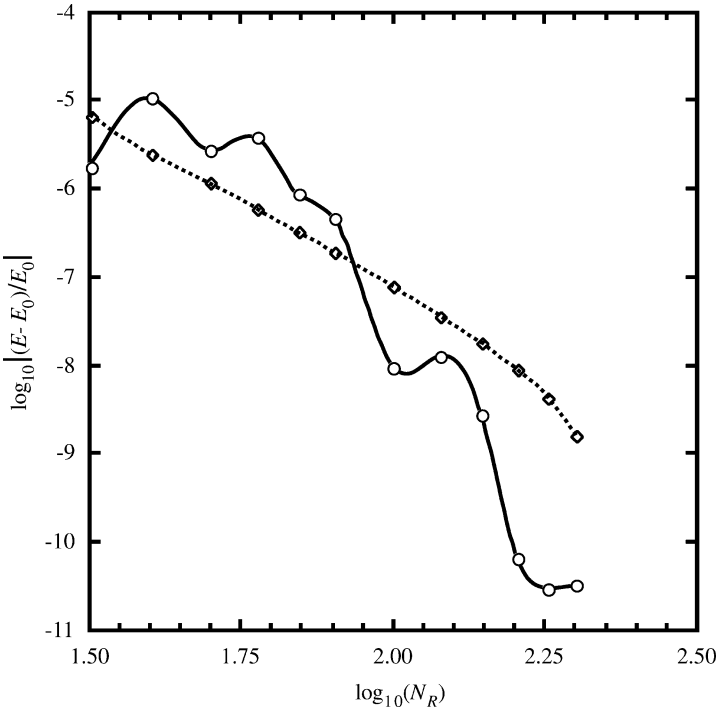

Fig. 3. Log_{10} of the relative error, $|(E - E_0)/E_0|$, for the energy of the lowest eigenvalue as a function of $\log_{10}$ of the number of radial grid points. The solid line with open circles was obtained for a potential in which the smooth radial kernel was used to interpolate the radial coordinate, where $E_0 = -445.769718711331\ \mathrm{cm}^{-1}$ is the value of E when $\log_{10}(N_R) = 2.3424$. The dotted line with open diamonds was for a potential in which the unsmooth radial kernel was used, where $E_0 = -445.77760908907\ \mathrm{cm}^{-1}$ is also the value of E when $\log_{10}(N_R) = 2.3424$. For these two graphs, all the remaining parameters were fixed at the values showed in Table 2. The symbols indicate the actual points calculated.

tolerance (E_τ) by taking the relative difference $|(E_\tau - E_0)/E_0|$. In Fig. 5, a plot on a logarithmic scale of the relative difference $|(E_\tau - E_0)/E_0|$ for the lowest energy eigenvalue as a function of $\log_{10}(\tau)$ is presented. As can be seen from Fig. 5, the negative of $\log_{10}|(E_\tau - E_0)/E_0|$ is related to the negative of $\log_{10}(\tau)$ by a linear relation. This clearly indicates that the relative uncertainty $|(E_\tau - E_0)/E_0|$ in the calculation of the energy of the lowest eigenvalue as a function of $\log_{10}(\tau)$ follows a linear relationship. This observation is quite interesting since it implies that keeping all the remaining parameters fixed, we can predict what the accuracy would be using a given tolerance, or we can predict the tolerance needed to compute the energy of the desired eigenvalue with the given accuracy.

After all parameters were optimized, the total number of 34,816 spectral basis functions were used. To examine the rate of convergence of the Lanczos method, we have also plotted in Fig. 6, the negative of $\log_{10}|(E_N - E_0)/E_0|$ vs the number of iterations N. From Fig. 6 can be seen that the relation between the number of iterations (N) and the negative of $\log_{10}|(E_N - E_0)/E_0|$ is linear. This behavior implies that the energy of the lowest eigenvalue converges exponentially with respect to the number of iterations (N).

6. Conclusions

The pseudo-spectral Lanczos method discussed in this paper can be used to calculate rovibrational energy levels of relatively weakly bound vdW dimers such as $(HX)_2$ (X = F, Br). For the $(HBr)_2$ dimer, the eigenvalues of the

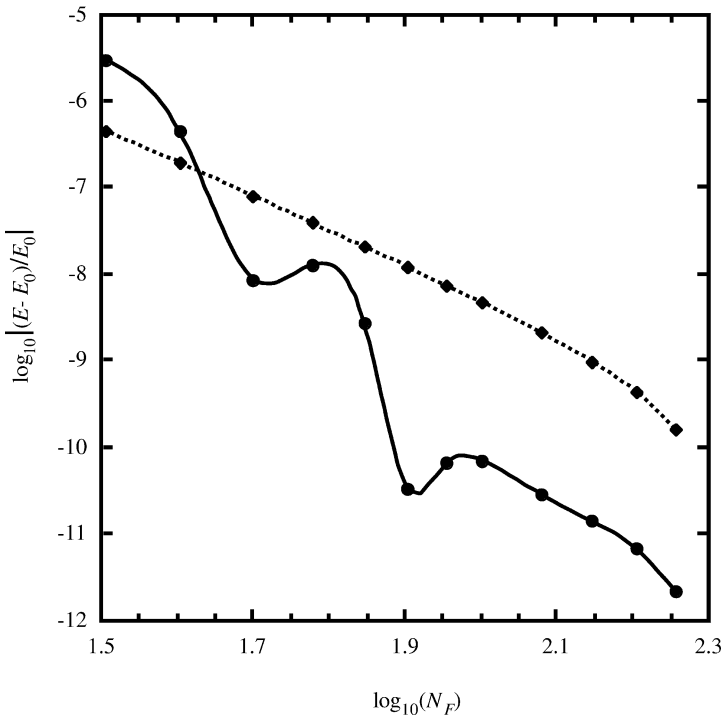

Fig. 4. Log_{10} of the relative error, $|(E - E_0)/E_0|$, for the energy of the lowest eigenvalue as a function of $\log_{10}$ of the number radial functions. The solid line with black circles, was obtained for a potential in which the smooth radial kernel was used to interpolate the radial coordinate, where $E_0 = -445.76972247153$ cm^{-1} is the value of E when $\log_{10}(N_F) = 2.30103$. The dotted line with black diamonds is for a potential in which the unsmooth radial kernel was used, where $E_0 = -445.77761157781$ cm^{-1} is also the value of E when $\log_{10}(N_F) = 2.30103$. For these two graphs, the N_R and N_F are related by $N_F = N_R/2$, all the remaining parameters were fixed at the values showed in Table 2. The symbols indicate the actual points calculated.

lowest total angular momentum, $J = 0$, were calculated, where, $j_{\max}$, the monomer rotational quantum number can take values between 8 and 10, and the grid representations used involves $N_R = 35$, $N_\theta = 12$ and $N_\phi = 17$ points. With these modest requirements, converged eigenvalues with uncertainties of ± 0.01 cm^{-1} were obtained. Analysis of the convergence properties of the eigenvalues calculated reveals that the convergence of the eigenvalues was exponential with respect to the number of iterations N. This is a particularly interesting result, which implies that the eigenvalues converge rapidly as the number of iterations increases, making this method suitable to calculate rovibrational energy levels of more complicated polyatomic vdW systems. The uncertainty of the eigenvalues, calculated as a function of tolerance, follows a linear relationship. This suggests that before calculations of a desired eigenvalue are carried out, since an estimate of the uncertainties of the eigenvalues to be calculated can be made.

The use of the least-squares interpolation method to obtain a global representation of the intermolecular potential of two-interacting linear rigid rotors, has been found to be a useful approach. In the application of this technique to the fitting of the potential of the $(HBr)_2$ dimer, the use of the switching functions to smooth the radial reproducing kernel, improves the smoothness of the potential along this coordinate. Comparison of the convergence for the energy of the lowest eigenvalue, as a function of the number of radial grid points and basis functions using the smooth and the unsmooth potential, demonstrates that the rate of convergence can be increased with the use of the smoothed potential. However, we also note that the use of the smoothed radial functions does lead to undesirable oscillatory behavior, but it still leads to better convergence than the use of unsmoothed radial functions.

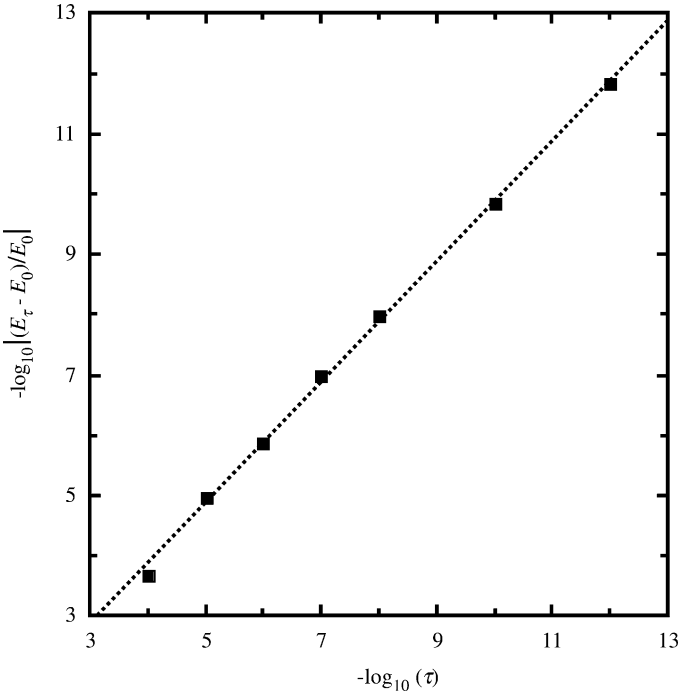

Fig. 5. The negative of $\log_{10}$ of the relative difference $|(E_\tau - E_0)/E_0|$, for the energy of the lowest eigenvalue ($J = 0$) of the $(HBr)_2$ dimer, as a function of the negative of $\log_{10}$ of the tolerance (τ).

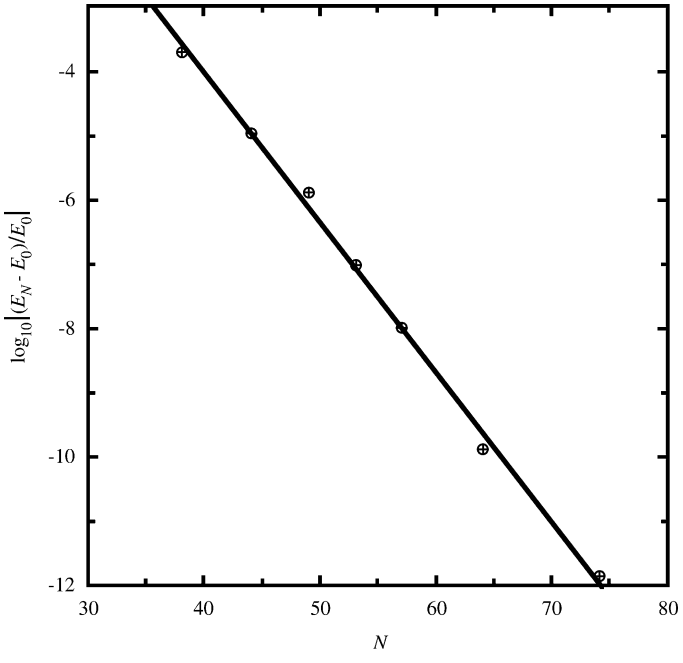

Fig. 6. $\mathrm{Log}_{10}|(E_\mathrm{N} - E_0)/E_0|$, the relative energy difference of the lowest eigenvalue ($J = 0$) of the $(HBr)_2$ dimer, as a function of the number of the iterations, N, in the Lanczos iterative procedure.

Acknowledgements

We gratefully acknowledge the financial support from the National Science Foundation, the Welch Foundation and the Texas Advanced Research Program. Finally, we also acknowledge the support of the Texas A&M University Supercomputing Facility.

References

[1] R.J. Le Roy, J.S. Carley, Adv. Chem. Phys. 42 (1980) 353.
[2] B. Carey, C.E. Chuaqui, K.G. Crowell, R.J. Le Roy, J. Chem. Phys. 105 (1996) 2639.
[3] M.J. Elrod, R.J. Saykally, J. Chem. Phys. 103 (1995) 933.
[4] M.J. Elrod, R.J. Saykally, J. Chem. Phys. 103 (1995) 921.
[5] A. van der Avoird, P.E.S. Wormer, R. Moszynski, in: S. Scheiner (Ed.), Molecular Interactions from van der Waals to Strongly Bound Complexes, John Wiley & Sons, Chichester, 1997, p. 105.
[6] G. Chalasinski, M. Szczesniak, Chem. Rev. 94 (1994) 1723.
[7] B. Jeziorski, R. Moszynski, K. Szalewicz, Chem. Rev. 94 (1994) 1887.
[8] X.T. Wu, A.B. McCoy, E.F. Hayes, J. Chem. Phys. 110 (1999) 2365.
[9] D.H. Zhang, Q. Wu, J.Z.H. Zhang, M. von Dirke, Z. Bačić, J. Chem. Phys. 102 (1995) 2315.
[10] M. Quack, M.A. Suhm, J. Chem. Phys. 95 (1991) 28.
[11] C.W. Necoechea, D.G. Truhlar, Chem. Phys. Lett. 224 (1994) 297.
[12] M.H. Alexander, A.E. DePristo, J. Chem. Phys. 65 (1976) 5009.
[13] P. Jensen, P.R. Bunker, A. Karpfen, M. Kofranek, H. Lischka, J. Chem. Phys. 93 (1990) 6266.
[14] M.J. Redmon, J.S. Binkley, J. Chem. Phys. 87 (1987) 969.
[15] P.R. Bunker, V.C. Epa, P. Jensen, A. Karpfen, J. Molec. Spectrosc. 146 (1991) 200.
[16] T.-S. Ho, T. Hollebeek, H. Rabitz, L.B. Harding, G.C. Schatz, J. Chem. Phys. 105 (1996) 10 472.
[17] T.-S. Ho, H. Rabitz, J. Chem. Phys. 104 (1996) 2584.
[18] G.C. Corey, D. Lemoine, J. Chem. Phys. 97 (1992) 4115.
[19] G.C. Corey, J.W. Tromp, J. Chem. Phys. 103 (1995) 1812.
[20] D. Lemoine, Comput. Phys. Commun. 97 (1996) 334.
[21] C. Leforestier, J. Chem. Phys. 101 (1994) 7357.
[22] C. Leforestier, L.B. Braly, K. Lui, M.J. Elrod, J. Saykally, J. Chem. Phys. 106 (1997) 8527.
[23] D. Kosloff, R. Kosloff, J. Comput. Phys. 47 (1982) 412.
[24] J.C. Light, I.P. Hamilton, J.V. Lill, J. Chem. Phys. 82 (1985) 1400.
[25] C.C. Corey, W.J. Tromp, in: C. Cerjan (Ed.), Numerical Grid Methods and Their Application to Schrödinger's Equation, Kluwer Academic, Boston, 1993, p. 1.
[26] D.O. Harris, G.G. Engerholm, W.D. Gwinn, J. Chem. Phys. 43 (1965) 1515.
[27] R.A. Friesner, J. Chem. Phys. 85 (1986) 1462.
[28] R.A. Friesner, M. Menou, C. Leforestier, J. Chem. Phys. 99 (1993) 324.
[29] G. Strang, Introduction to Applied Mathematics, Wellesley-Cambridge, Wellesley, 1986.
[30] J.K. Cullum, R.A. Willoughby, Lanczos Algorithms for Large Symmetric Eigenvalue Computations, Vols. 1 and 2, Birkhäuser, Boston, 1985.
[31] G. Brocks, A. van der Avoird, B.T. Sucliffe, J. Tennyson, Mol. Phys. 50 (1983) 1025.
[32] G.C. Gray, K.E. Gubbins, Theory of Molecular Fluids, Vol. I, Clarendon Press, Oxford, 1984.
[33] A. van der Avoird, P.E.S. Wormer, R. Szalewicz, Chem. Rev. 94 (1994) 1931.
[34] S. Green, J. Chem. Phys. 62 (1975) 2271.
[35] C. Cohen-Tannoudji, B. Diu, F. Laloe, Quantum Mechanics, Vol. I, Herman, Paris, France, 1977.
[36] J. Castillo-Chará, R.R. Lucchese, J.W. Bevan, J. Chem. Phys. (submitted).
[37] J.N. Murrell, S. Carter, S.C. Franatos, P. Huxley, A.J.C. Varandas, Molecular Potential Energy Surfaces, Wiley, Chichester, 1984.
[38] A.J. Rasmussen, K.E. Gates, S. Smith, J. Chem. Phys. 110 (1999) 1354.
[39] R.C. Cohen, R.J. Saykally, Ann. Rev. Phys. Chem. 42 (1991) 369.
[40] M.E. Rose, Elementary Theory of Angular Momentum, Wiley, New York, 1957.
[41] G. Danby, J. Phys. B 16 (1983) 3393.
[42] M. Abramowitz, I.A. Stegun, Handbook of Mathematical Functions, Dover, New York, 1964.
[43] C. Lanczos, J. Res. Natl. Bur. Stand. 45 (1950) 255.
[44] A.F.C. DeLucia, P. Helminger, W. Gordy, Phys. Rev. A 3 (1971) 1849.